JACS
JOURNAL OF THE AMERICAN CHEMICAL SOCIETY

Communication

pubs.acs.org/JACS

Catalytic Cycle of the *N*-Acetylglucosaminidase NagZ from *Pseudomonas aeruginosa*

Iván Acebrón,[†,§] Kiran V. Mahasenan,[‡,§] Stefania De Benedetti,[‡] Mijoon Lee,[‡] Cecilia Artola-Recolons,[†] Dusan Hesek,[‡] Huan Wang,[‡] Juan A. Hermoso,[*,†] and Shahriar Mobashery[*,‡]

[†]Department of Crystallography and Structural Biology, Institute of Physical Chemistry "Rocasolano", CSIC, 28006 Madrid, Spain
[‡]Department of Chemistry and Biochemistry, University of Notre Dame, Notre Dame, Indiana 46556, United States

Supporting Information

ABSTRACT: The *N*-acetylglucosaminidase NagZ of *Pseudomonas aeruginosa* catalyzes the first cytoplasmic step in recycling of muropeptides, cell-wall-derived natural products. This reaction regulates gene expression for the β-lactam resistance enzyme, β-lactamase. The enzyme catalyzes hydrolysis of *N*-acetyl-β-D-glucosamine-(1→4)-1,6-anhydro-*N*-acetyl-β-D-muramyl-peptide (**1**) to *N*-acetyl-β-D-glucosamine (**2**) and 1,6-anhydro-*N*-acetyl-β-D-muramyl-peptide (**3**). The structural and functional aspects of catalysis by NagZ were investigated by a total of seven X-ray structures, three computational models based on the X-ray structures, molecular-dynamics simulations and mutagenesis. The structural insights came from the unbound state and complexes of NagZ with the substrate, products and a mimetic of the transient oxocarbenium species, which were prepared by synthesis. The mechanism involves a histidine as acid/base catalyst, which is unique for glycosidases. The turnover process utilizes covalent modification of D244, requiring two transition-state species and is regulated by coordination with a zinc ion. The analysis provides a seamless continuum for the catalytic cycle, incorporating large motions by four loops that surround the active site.

The *Enterobacteriaceae* and *Pseudomonas aeruginosa* have devised an elaborate link between the complex process of cell-wall recycling and resistance to β-lactam antibiotics (Figure 1).[1] As the cell wall is damaged on exposure to the antibiotic, the organism attempts to repair it by removal of the damaged components and by *de novo* synthesis of cell wall. The removal of the damaged cell wall is instigated by the functions of lytic transglycosylases (LTs) within the periplasm.[2,3] The products of turnover of cell wall by these enzymes are referred to as muropeptides, as exemplified by compound **1**.[4−6] The AmpG permease internalizes the muropeptides, which undergo further processing in the cytoplasm by enzymes NagZ and AmpD, en route to the formation of Lipid II (**6**), which is put to the surface of the membrane for the *de novo* biosynthetic process[7] in the recycling arm of the system. Both muropeptides **1** and **3**, in their pentapeptide versions, bind to the transcriptional regulator AmpR in a process that activates transcription of the gene *ampC* for the class C β-lactamase, the major resistance determinant to β-lactam antibiotics in these organisms.[8]

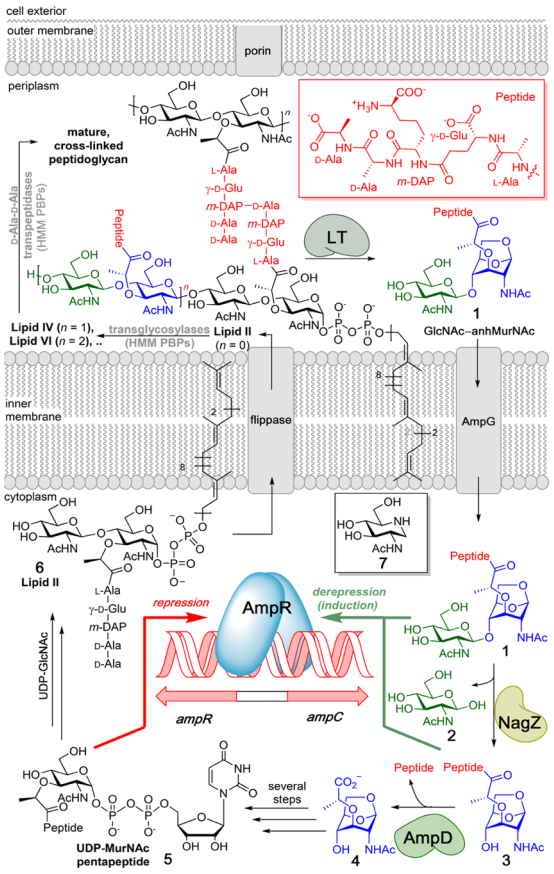

Figure 1. Cell-wall recycling in Gram-negative bacteria with NagZ as the first cytoplasmic step. Compound **7** is a potent inhibitor of NagZ. The structure of the full-length stem pentapeptide is given in a box in the upper right corner.

The reaction of the *N*-acetylglucosaminidase NagZ (Figure 1) is the first cytoplasmic committed step in the recycling process.[3,9−11] In the present report, we describe the catalytic cycle of NagZ from *P. aeruginosa* by a collection of seven X-ray structures, three computational models, molecular-dynamics simulations, and site-directed mutagenesis. Several species in the catalytic cycle were synthetically prepared for investigation of the

Received: February 15, 2017
Published: May 8, 2017

ACS Publications © 2017 American Chemical Society

DOI: 10.1021/jacs.7b01626
J. Am. Chem. Soc. 2017, 139, 6795−6798

incremental steps in substrate turnover. We also document that catalysis by this enzyme entails dramatic conformational changes, which were captured by the X-ray structures and the simulations in defining the enzymatic reaction.

The *nagZ* gene from *P. aeruginosa* PAO1 was cloned and expressed and the protein was purified to homogeneity, as we reported earlier.[12] Crystallization was accomplished by the sitting-drop vapor-diffusion method under 30% PEG 8000, 100 mM sodium cacodylate pH 6.0, and 200 mM sodium acetate, pH 6.0. NagZ is a 36.1 kDa protein comprised of a single domain with a TIM-barrel fold. The wild-type apo enzyme structure was determined at 1.8-Å resolution (Figure 2, Figure 3A, Figure S1A, and Table S1). The protein is a compact structure of 56 Å × 50 Å × 40 Å with the active site located at the center of the β-barrel, surrounded by five loops, L1−L5 (Figure 2). In the apo state, H174 is distant from the active site and D244 is buried into the protein core. As we will describe, upon constitution of the active site, three loops converge to form segments of the active site. The active-site residues R131 (on L2), H174 (on L3), and D244 (on L5) experience dramatic motions of 25 Å, 12 Å, and 6 Å, respectively (Figure 2). Mutations of these amino acids rendered the enzyme inactive, so they are critical (Table S2). A 1-μs molecular-dynamics (MD) simulation with AMBER14[13] demonstrated the propensity of the L2-loop to approach the catalytic site. To sample the full conformational motion of L2-loop, a targeted-molecular-dynamics (TMD) calculation was performed (Supporting Information). The X-ray structure of the open apo state (Figure 3A) and that of the product-bound complex (discussed in Figure 3G; representing an active site that is constituted) provided the starting and the end points, respectively. R131 (on L2) sampled a series of salt-bridge interactions with neighboring residues, and bringing F133 into a hydrophobic pocket, before arriving at the final state spanning the 25-Å distance (Movie S1). Importantly, mutation at F133 resulted in loss of activity (Table S2), revealing the critical role of the residue in recognition at the hydrophobic pocket, which directs the loop into the suitable conformation for catalysis.

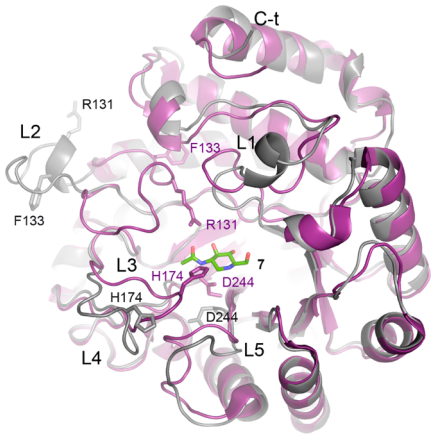

Figure 2. Overview of the structural changes upon ligand binding by NagZ. Structural superimposition of the apo NagZ (gray) and the NagZ:7 complex (magenta). Catalytic residues H174 and D244, together with the critical R131 and F133 are shown in capped sticks. Inhibitor 7 is represented in green capped sticks for its carbon atoms. Loops around active site are labeled. Similar changes (except for L3) are observed for the NagZ:**2** and the NagZ:**2**:**3** complexes.

We generated a model of the catalytically competent substrate-bound state (Figure 3B) based on the X-ray structure of NagZ bound with inhibitor **7** (Figure 3C, discussed below). We used the Glide program (v 5.5, Schrodinger LLC, NY) for docking of the substrate (**1**), guided by the X-ray positions seen for products **2** and **3** (Figure 3F). The complex was placed in a box of TIP3P water molecules, energy-minimized, and subjected to MD simulations. The constituted active site of the inhibitor-bound X-ray complex was nicely poised to accommodate the substrate straddling the −1 and +1 subsites, whereas the peptide stem of the substrate was mostly exposed to the solvent. We observed favorable hydrogen bonding by H174 with the glyosidic oxygen atom of **1**, a step critical for its protonation for bond scission (discussed below).

2-Acetamido-1,2-dideoxynojirimycin (**7**), synthesized in 13 steps by a known method,[12] is a mimetic of the transient oxocarbenium species in the course of the conversion of muropeptide **1** to products **2** and **3** by NagZ (Figure 3C,D). Compound **7** inhibits NagZ with a K_i of 300 ± 15 nM.[12] The structure of the complex of this inhibitor bound to NagZ was solved at 3.1-Å resolution (Figure 3C and Table S1). The electron density for the inhibitor is clearly seen in the active site (Figure S2A). Loops L2, L3, and L5 converge onto the active site to bring residues R131, H174, and D244, respectively, to within the contact shell of the inhibitor (as depicted in the lower panel of Figure 3C for the high-energy species of the reaction). The side chain of R131 (L2-loop, Figure 2) hydrogen bonds consistently to carbonyl of the acetamido group of *N*-acetylglucosamine in structures of Figure 3B−D and continues to do so in those of Figure 3E−G (not shown graphically). Its function would appear to be anchoring of the *N*-acetylglucosamine at the −1 subsite of the active site. We note that H174 (L3-loop, Figure 2) in the X-ray is now poised to within hydrogen-bonding distance to the glycosidic oxygen of the substrate (as in Figure 3B). Protonation of the glycosidic oxygen by H174 facilitate its departure. In the model for the substrate-bound state (Figure 3B), H174 hydrogen bonds with the neighboring Asp172, forming what Litzinger et al. noted as a catalytic dyad.[10] It is noteworthy that orientation of L3 toward the inhibitor is not driven by H174, as mutation to Ala at this position provides the same 3D structure (Figure S3). The position of the inhibitor (**7**) in the X-ray is superimposable to that of *N*-acetylglucosamine (**2**), which would come from the substrate (Figure 3B). We also note that D244 (L5-loop, Figure 2) in the X-ray is now nicely positioned (Figure 3C) to covalently link to C1 of *N*-acetylglucosamine (in the substrate) to give the ester intermediate (Figure 3C,D), which was seen by Bacik et al. for the NagZ from *Salmonella typhimurium*.[11] The distance between the D244 side-chain oxygen to C1 of the inhibitor, the site of covalent attachment to the *N*-acetylglucosamine in the substrate, is 3.3 Å. The D244 side chain is indisposed for interaction when the substrate binds, but the incipient and transient formation of the oxocarbonium ion would electrostatically assist its rotation toward the anomeric carbon for covalent attachment. The nucleophilic attack of D244 on the anomeric carbon results in the formation of product **3** and the covalent glycosyl-enzyme intermediate. A model of this stage of the catalytic cycle (Figure 3D) was generated based on our inhibitor-bound complex (Figure 3C), also incorporating insights from two additional X-ray structures. The position of **3** was modeled based on our structure of NagZ in complex with the two products (Figure 3F). The X-ray structure of ester intermediate[11] (mentioned above) guided the way for building the glycosyl-enzyme species model. The model was immersed in a box of TIP3P water molecules and was energy minimized with

DOI: 10.1021/jacs.7b01626
J. Am. Chem. Soc. 2017, 139, 6795−6798

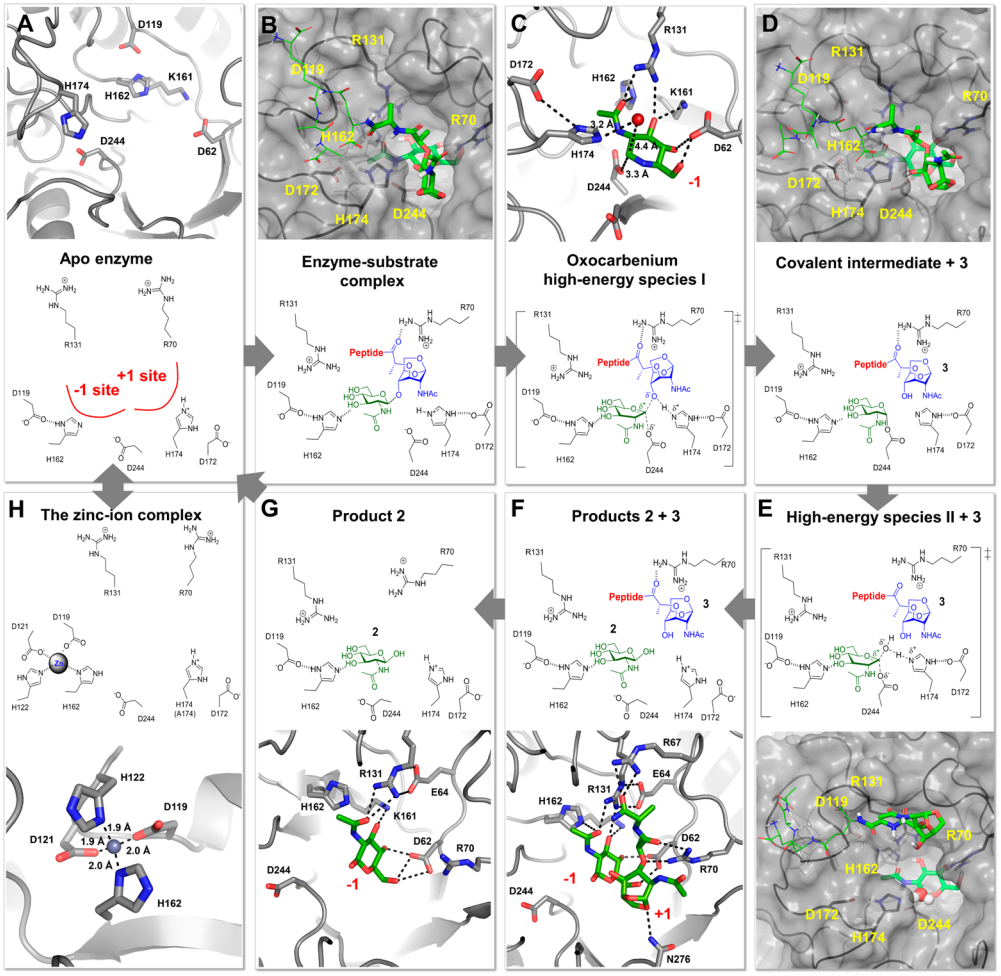

Figure 3. Steps in the catalytic cycle of NagZ are depicted based on the X-ray crystal structures and computational models based on the crystallographic information (the gray translucent Connolly surfaces). (A) Apo NagZ seen with an "open" active site. (B) Computational model for the enzyme–substrate complex based on the X-ray structures of panels C and F, and a previously reported X-ray structure.[11] (C) X-ray structure of the complex of inhibitor **7** with NagZ shows a fully constituted active site. With **7** as a mimetic of the oxocarbenium species, the transition-state for the glycosidic-bond scission is shown. (D) Computational model of the covalently bound *N*-acetylglucosamine and the product **3**. (E) Snapshot of the molecular-dynamics simulation of the complex in panel D shows a water molecule (at 5 o'clock) entering the active site and positioned between C1 of *N*-acetylglucosamine and the side chain of H174 (Movie S2). (F) X-ray structure of products **2** and **3** bound to the active site. (G) X-ray structure of product **2** within the active site (H) Zinc-ion-inhibited NagZ (H174A mutant) shows tetrahedral coordination of zinc ion by four residues, of which three, D119, H122, and D121 are located on the L2-loop. This coordination locks the L2-loop away from the active site. The orientations of the chemical structures and the graphics in each panel are not the same for the clarity of representation. See Figure S1 for stereo view of the above panels.

the PMEMD module of AMBER14 (Figure 3D). The covalent *N*-acetylglucosamine-enzyme species is essentially that seen in the X-ray structure,[11] except our complex also has the information on binding of **3** at the +1 subsite. Notwithstanding that **3** was seen hydrogen bonded to the side chain of R70 (Figure 3F), this interaction is not critical as the R70A mutant retained catalytic activity (Table S2). At approximately 50 ns of dynamics simulations of the model of Figure 3D, a water molecule from the milieu inserted into the active site between H174 (2.9 Å) and C1 (3.4 Å) of the covalently bound *N*-acetylglucosamine (Movie S2). This placement enables activation of the water molecule by the D172-H174 dyad for nucleophic attack at the C1 carbon, which would displace D244, as proposed first by Vocadlo et al.[14] It is noteworthy that this exact same position is seen occupied by a water molecule in the X-ray structure with inhibitor **7** (Figure 3C). Hence, the mechanistic importance of this specific water molecule is underscored by the fact that the constituted active site has a binding pocket for it. The presence of the second ring in the high-energy species depicted in Figure 3C abrogates the opportunity for the water molecule to occupy the active site. However, once product **2** is relocated on breakage of the glycosidic bond, it becomes possible again (Figure 3D,E; Movie S2). The position of inhibitor **7** (as a mimetic of the oxocarbenium species in the transition state), aligned with the nucleophilic water molecule and the side chain of H174 are seen seamlessly with continuous electron density (Figure S2A). The now-free-base H174 activates the water molecule for displacement of D244. The second transition-state species depicted in Figure 3E is based also on the X-ray structure described in Figure 3C, as both involve the transient oxocarbenium species.

Next, crystals of the wild-type NagZ were soaked overnight with a synthetic sample of the substrate **1**. Muropeptide **1** was prepared in 44 synthetic steps for this study, per a reported method.[15] The complex that resulted was that of NagZ with the two products of turnover, compounds **2** and **3**, at 2.18-Å resolution (Figure 3F and Table S1); the reaction had taken place within the crystal. H174, having completed its catalytic

DOI: 10.1021/jacs.7b01626
J. Am. Chem. Soc. 2017, 139, 6795–6798

function(s) had moved away by as much as 13 Å in this complex. Interestingly, we observed a tendency of H174 to flip out in our previous MD simulation of the covalent intermediate (Movie S2). D244 relocated by as much as 5.5 Å and is buried back into the protein core. There was clear density for both products within the active site (except for the segments of the mobile peptide stem on **3**; Figure S2B), and notable changes that were observed in crystallographic B-factors (Figure S4). In a second soaking of the wild-type NagZ with **1**, we obtained the complex in Figure 3G at 3.0-Å resolution (Table S1), where after catalysis only the noncovalently bound *N*-acetylglucosamine (**2**) was seen in the active site (Figure S2C). Compound **3** had already diffused away from the active site, and as a consequence R70 also had repositioned, as it no longer had **3** (or the substrate) to hydrogen-bond with at the +1 subsite. The departure of product **3** from the complex of Figure 3G brings the structure of NagZ back to that of the apo structure, as depicted in Figure 3A.

The conformation of the saccharide in **3**, as shown in the X-ray structure of Figure 3F, is of special interest. The density fits only to the $B_{3,O}$ (boat) conformer, which is a few kcal/mol higher in energy than the $^1C_4$ (chair) conformer, which is seen in solution.[4] The relaxation of the structure from $B_{3,O}$ to $^1C_4$ might be the impetus for expulsion of **3** from the active site, as the peptide in **3** would have steric clashes within the complex in the more stable conformer.

In the course of our studies, we also had made the H174A mutant NagZ. This protein crystallized at 2.15-Å resolution (Table S1), but when the structure was solved, we were surprised to find the protein coordinated by a zinc ion in a distinctly new conformational state. This structure entailed a drastic conformational change in the L1 and L2 loops, whereby R131 had relocated away from the active site (Movie S3, and Figure S5). The zinc ion is tetrahedrally coordinated by D119, D121, H122, and H162 with distances close to 2 Å (Figure 3H). H162 is an active-site residue because it hydrogen bonds to both the substrate and product **3**. The coordination was confirmed by measurement of the zinc-ion anomalous signal at synchrotron radiation facility and by the unequivocal electron density for it (Figure S2D). The inhibitory role of the zinc ion was confirmed experimentally by measurement of the dissociation constant for binding of the zinc ion to wild-type NagZ at 320 ± 50 nM by an activity assay. The inhibition was reversed by incubation with a chelating agent (EDTA). Furthermore, we demonstrated by crystallographic experiments that zinc-ion chelation by EDTA reverted the structure to that of the apo wild-type NagZ (Figure S6 and Table S1). Intracellular concentration of free zinc ion in bacteria is reported to be low (femtomolar to picomolar) and tightly controlled by various mechanisms.[16] Hence, how and what might regulate the NagZ activity by zinc-ion coordination or even its relevance in biology of Gram-negative bacteria is not understood.

We have described here the catalytic cycle of NagZ from *P. aeruginosa*, which entails conformational changes by the loops surrounding the active site. It is likely that the trigger for the conformational change is occupancy (by substrate) within the active site. NagZ serves as a case study in dramatic conformational changes in catalysis by an enzyme.

■ ASSOCIATED CONTENT

Supporting Information

The Supporting Information is available free of charge on the ACS Publications website at DOI: 10.1021/jacs.7b01626.

Methods of X-ray crystallography, site-directed mutagenesis, computational analysis, and additional figures (PDF)

Targeted molecular-dynamics simulation of the transition of L2-loop (AVI)

Molecular-dynamics simulation of a model of the glycosyl-enzyme species (AVI)

Morph animation of the structural changes seen with zinc inhibition of NagZ (AVI)

■ AUTHOR INFORMATION

Corresponding Authors

*mobashery@nd.edu

*xjuan@iqfr.csic.es

ORCID

Shahriar Mobashery: 0000-0002-7695-7883

Author Contributions

[§]The first two authors contributed equally to this work.

Notes

The authors declare no competing financial interest.

■ ACKNOWLEDGMENTS

This work in the USA was supported by a grant from the NIH (GM61629) and in Spain by a grant from the Spanish Ministry of Economy and Competitiveness (BFU2014-59389-P). We thank the staff from ALBA, ESRF and SLS synchrotrons for help in X-ray data collection and assistance by the Center for Research Computing (CRC) of the University of Notre Dame for the computing resources.

■ REFERENCES

(1) Fisher, J. F.; Mobashery, S. *Bioorg. Chem.* **2014**, *56*, 41.

(2) Cho, H.; Uehara, T.; Bernhardt, T. G. *Cell* **2014**, *159*, 1300.

(3) Johnson, J. W.; Fisher, J. F.; Mobashery, S. *Ann. N. Y. Acad. Sci.* **2013**, *1277*, 54.

(4) Lee, M.; Zhang, W.; Hesek, D.; Noll, B. C.; Boggess, B.; Mobashery, S. *J. Am. Chem. Soc.* **2009**, *131*, 8742.

(5) Lee, M.; Dhar, S.; De Benedetti, S.; Hesek, D.; Boggess, B.; Blazquez, B.; Mathee, K.; Mobashery, S. *Angew. Chem., Int. Ed.* **2016**, *55*, 6882.

(6) Lee, M.; Hesek, D.; Dik, D. A.; Fishovitz, J.; Lastochkin, E.; Boggess, B.; Fisher, J. F.; Mobashery, S. *Angew. Chem., Int. Ed.* **2017**, *56*, 2735.

(7) Silhavy, T. J.; Kahne, D.; Walker, S. *Cold Spring Harbor Perspect. Biol.* **2010**, *2*, a000414.

(8) Dik, D. A.; Dominguez-Gil, T.; Lee, M.; Hesek, D.; Byun, B.; Fishovitz, J.; Boggess, B.; Hellman, L. M.; Fisher, J. F.; Hermoso, J. A.; Mobashery, S. *J. Am. Chem. Soc.* **2017**, *139*, 1448.

(9) Balcewich, M. D.; Stubbs, K. A.; He, Y.; James, T. W.; Davies, G. J.; Vocadlo, D. J.; Mark, B. L. *Protein Sci.* **2009**, *18*, 1541.

(10) Litzinger, S.; Fischer, S.; Polzer, P.; Diederichs, K.; Welte, W.; Mayer, C. *J. Biol. Chem.* **2010**, *285*, 35675.

(11) Bacik, J. P.; Whitworth, G. E.; Stubbs, K. A.; Vocadlo, D. J.; Mark, B. L. *Chem. Biol.* **2012**, *19*, 1471.

(12) Yamaguchi, T.; Blazquez, B.; Hesek, D.; Lee, M.; Llarrull, L. I.; Boggess, B.; Oliver, A. G.; Fisher, J. F.; Mobashery, S. *ACS Med. Chem. Lett.* **2012**, *3*, 238.

(13) Case, D. A., et al. University of California, San Francisco, 2014.

(14) Vocadlo, D. J.; Mayer, C.; He, S.; Withers, S. G. *Biochemistry* **2000**, *39*, 117.

(15) Hesek, D.; Lee, M.; Zhang, W.; Noll, B. C.; Mobashery, S. *J. Am. Chem. Soc.* **2009**, *131*, 5187.

(16) Watly, J.; Potocki, S.; Rowinska-Zyrek, M. *Chem. - Eur. J.* **2016**, *22*, 15992.

DOI: 10.1021/jacs.7b01626
J. Am. Chem. Soc. 2017, 139, 6795−6798